

# Spherical collapse of dark energy with an arbitrary sound speed

Tobias Basse<sup>1</sup>, Ole Eggers Bjælde<sup>1,2</sup> and Yvonne Y. Y. Wong<sup>2</sup>

<sup>1</sup> Department of Physics and Astronomy, Aarhus University, Ny Munkegade 120, DK-8000 Aarhus C, Denmark

<sup>2</sup> Institut für Theoretische Teilchenphysik und Kosmologie  
RWTH Aachen, D-52056 Aachen, Germany

E-mail: [tb06@phys.au.dk](mailto:tb06@phys.au.dk), [oeb@phys.au.dk](mailto:oeb@phys.au.dk),  
[yvonne.wong@physik.rwth-aachen.de](mailto:yvonne.wong@physik.rwth-aachen.de)

**Abstract.** We consider a generic type of dark energy fluid, characterised by a constant equation of state parameter  $w$  and sound speed  $c_s$ , and investigate the impact of dark energy clustering on cosmic structure formation using the spherical collapse model. Along the way, we also discuss in detail the evolution of dark energy perturbations in the linear regime. We find that the introduction of a finite sound speed into the picture necessarily induces a scale-dependence in the dark energy clustering, which in turn affects the dynamics of the spherical collapse in a scale-dependent way. As with other, more conventional fluids, we can define a Jeans scale for the dark energy clustering, and hence a Jeans mass  $M_J$  for the dark matter which feels the effect of dark energy clustering via gravitational interactions. For bound objects (halos) with masses  $M \gg M_J$ , the effect of dark energy clustering is maximal. For those with  $M \ll M_J$ , the dark energy component is effectively homogeneous, and its role in the formation of these structures is reduced to its effects on the Hubble expansion rate. To compute quantitatively the virial density and the linearly extrapolated threshold density, we use a quasi-linear approach which is expected to be valid up to around the Jeans mass. We find an interesting dependence of these quantities on the halo mass  $M$ , given some  $w$  and  $c_s$ . The dependence is the strongest for masses lying in the vicinity of  $M \sim M_J$ . Observing this  $M$ -dependence will be a tell-tale sign that dark energy is dynamic, and a great leap towards pinning down its clustering properties.

## 1. Introduction

The apparent accelerating expansion of our universe is, according to the standard model of cosmology, best described by the presence of a dark energy component with a strong negative pressure, dominating the gravitational physics on large scales (see, e.g., [1–3] for reviews). However, our knowledge of the actual properties of this dark energy is very limited, and a number of open questions remain—Is dark energy dynamic or not? Does it take part in clustering? Is the dark energy’s behaviour scale-dependent?—to name but a few.

In order to distinguish between various models of dark energy, we must appeal to a variety of observational tests, each probing a different aspect of the dark energy’s dynamics. Luminosity and angular diameter distance measurements using, respectively, type Ia supernovae and the baryon acoustic oscillation scale have yielded—and will continue to yield—interesting information on the dark energy’s influence on the expansion history of the universe. The cosmic microwave background temperature anisotropies [4–8], as well as their cross-correlations with tracers of the large-scale structure distribution [9–12], provide a means to track the dark energy’s impact on the evolution of the gravitational potential via the late integrated Sachs–Wolfe effect. Weak gravitational lensing of distant objects probes the dark energy’s effect on the distance–redshift relation and the growth function [13–15]. Lastly, the formation of gravitationally bound objects such as galaxies and galaxy clusters is also sensitive to the detailed properties of the dark energy component [16–19].

Into the last category falls the so-called spherical collapse model [20], which, as the name suggests, is a model of gravitational collapse simplified by the assumption of spherical symmetry. In the model, a spherically symmetric overdense region with uniform density evolves to a configuration of infinite density under its own gravity, and a gravitationally bound object is said to be formed.

The original spherical collapse model was constructed under the assumption of an Einstein–de Sitter (EdS) universe. Already by the 1980s and the early 1990s the model had been extended to include a cosmological constant [21–23], and later for quintessence [24]. More analyses have followed since then, and all reached the conclusion that dark energy has an important impact on the formation of gravitationally bound structures [25–28]. The topic appears to have gained momentum again during the past year [29–34] mainly because of the positive expectation that these results will be testable against observations in the not-too-distant future [35].

In this paper we investigate by means of the spherical collapse model how a generic dark energy component characterised by a constant equation of state parameter  $w < -1/3$  and sound speed  $c_s$  affects the formation of cosmic structures. In previous studies the dark energy component is generally allowed to take on different values of  $w$ . However, the sound speed  $c_s$  is invariably assumed to be either approaching the speed of light so that the dark energy is essentially homogeneous, or exactly vanishing so that the dark energy fluid is comoving with the matter component. These assumptions

undoubtedly simplify the calculations considerably and represent the two limiting behaviours of dark energy clustering. However, the case of a general sound speed remains interesting in that it introduces a scale-dependence into the problem. Identifying this dependence will give us yet another pointer to the true nature of dark energy. Here, we demonstrate for the first time how to incorporate a dark energy component with an arbitrary sound speed into the spherical collapse model (in an approximate way).

The paper is organised as follows. In section 2 we introduce the evolution equations for the spherical collapse and the corresponding equations of motion for the dark energy component. In section 3 we discuss dark energy clustering within the framework of linear perturbation theory. Section 4 contains our numerical results. Our conclusions are presented in section 5.

## 2. Spherical collapse

### 2.1. The spherical top hat and equations of motion for the matter component

In its most basic formulation, the spherical collapse model assumes there exists a spherically symmetric overdense region on top of an otherwise uniform background matter density field. The overdense region is characterised by a physical radius  $R_i \equiv R(\tau_i)$  at the initial (conformal) time  $\tau_i$ , and a uniform initial energy density

$$\rho_m^{\text{th}}(\tau_i) \equiv \bar{\rho}_m(\tau_i)(1 + \delta_{m,i}^{\text{th}}), \quad (2.1)$$

where  $\bar{\rho}_m(\tau)$  denotes the energy density of the background matter field. This is our spherical “top hat” perturbation, and the mass contained within is given by

$$M = \frac{4\pi}{3} \bar{\rho}_m(\tau_i)(1 + \delta_{m,i}^{\text{th}})R_i^3 = \frac{4\pi}{3} \bar{\rho}_m(\tau_0)(1 + \delta_{m,i}^{\text{th}})X_i^3, \quad (2.2)$$

where  $\tau_0$  denotes the present time, and we have defined

$$X \equiv \frac{R}{a} \quad (2.3)$$

as the comoving radius of the top hat.

The evolution of the physical top hat radius  $R$  with respect to *cosmic time*  $t$  is described by the familiar equation of motion

$$\frac{1}{R} \frac{d^2 R}{dt^2} = -\frac{4\pi G}{3}(\rho_m^{\text{th}} + \rho_Q^{\text{th}} + 3P_Q^{\text{th}}), \quad (2.4)$$

where we have incorporated in the equation the possibility of a second energy component with a nonzero pressure denoted by the subscript  $Q$ . This second component is uniform inside the top hat region defined by the radius  $R$ , and shall be our dark energy component in this work. Equation (2.4) can be equivalently expressed as an equation of motion for the comoving top hat radius  $X$  with respect to conformal time  $\tau$ ,

$$\frac{\ddot{X}}{X} + \mathcal{H} \frac{\dot{X}}{X} = -\frac{4\pi G}{3}a^2[\bar{\rho}_m\delta_m^{\text{th}} + \bar{\rho}_Q(1 + 3c_s^2)\delta_Q^{\text{th}}], \quad (2.5)$$

where  $\cdot \equiv \partial/\partial\tau$ ,  $\mathcal{H} = aH$  is the conformal Hubble parameter, and

$$c_s^2 \equiv \left. \frac{\delta P_Q}{\delta \rho_Q} \right|_{\text{rest}} \quad (2.6)$$

is the square of dark energy sound speed defined in the dark energy fluid's rest frame. Note that in identifying  $c_s$  in equations (2.5) and (2.6) as the rest frame sound speed, we have implicitly assumed that we are dealing only with length scales much smaller than the Hubble length, and that averaged over the spherical region, there is no bulk flow of dark energy relative to the dark matter fluid. We also assume  $c_s^2$  to be constant in time and space.

Since the total mass of matter inside the top hat  $M = (4\pi/3)\rho_m^{\text{th}}R^3$  is conserved, the top hat matter density contrast  $\delta_m^{\text{th}}$  can be easily expressed as a function of the top hat radius,

$$\begin{aligned} \delta_m^{\text{th}}(\tau) &\equiv \frac{\rho_m^{\text{th}}(\tau)}{\bar{\rho}_m(\tau)} - 1 \\ &= (1 + \delta_{m,i}^{\text{th}}) \left[ \frac{a(\tau)}{a(\tau_i)} \frac{R_i}{R(\tau)} \right]^3 - 1 = (1 + \delta_{m,i}^{\text{th}}) \left[ \frac{X_i}{X(\tau)} \right]^3 - 1. \end{aligned} \quad (2.7)$$

For the dark energy density contrast  $\delta_Q^{\text{th}}$ , two limiting cases have been studied in the literature. The first is the non-clustering limit, in which the dark energy sound speed  $c_s$  is taken to approach the speed of light, see e.g. [24]. In this case,  $\delta_Q^{\text{th}}$  is effectively zero, so that the role of dark energy in the spherical collapse enters only through the Hubble expansion of the background.‡

The second is the “comoving” or clustering limit, in which the dark energy sound speed is exactly zero, see e.g. [31]. As we shall see in the next section, the Euler equation for the dark energy fluid in this limit is identical to its counterpart for a nonrelativistic dark matter fluid. This means that the bulk velocity fields of the two fluids are the same; the fluids are thus said to be comoving. Note that this observation does not imply the dark energy and dark matter density contrasts evolve in the same manner, since the conditions for energy conservation differ between the two fluids. It does, however, imply a conservation law for the dark energy component inside the top hat, so that the evolution of  $\rho_Q^{\text{th}}$  can be simply expressed as

$$\frac{d\rho_Q^{\text{th}}}{dt} + \frac{3}{R} \frac{dR}{dt} (\rho_Q^{\text{th}} + \bar{P}_Q) = 0, \quad (2.8)$$

or

$$\dot{\rho}_Q^{\text{th}} + 3 \left( \mathcal{H} + \frac{\dot{X}}{X} \right) (\rho_Q^{\text{th}} + \bar{P}_Q) = 0 \quad (2.9)$$

in terms of comoving quantities.

Strictly speaking, these two limiting cases are the only ones for which the top hat formulation is exact. The case of an arbitrary dark energy sound speed  $c_s$  is

‡ Note that in order to get exactly zero dark energy clustering, the sound speed would have to be infinite; See the linear solutions (3.4) and (3.6).

strictly not amenable to this simple treatment, since the existence of a finite sound speed and therefore the provision for the propagation of sound waves imply that the energy densities—both dark matter and dark energy—inside the overdense region must evolve to a nonuniform configuration, even if they are initially uniform. Having said this, however, we must also bear in mind that the spherical collapse model is itself a simplified model of structure formation, and the top hat density contrast should be interpreted as the average density contrast inside a region after a unit top hat filtering function has been applied. If we take this as our guiding principle, then the generalisation of the spherical top hat to include a dark energy component with an arbitrary sound speed simply requires that we interpret  $\delta_Q^{\text{th}}$  as the spatially averaged density contrast of the dark energy field inside a region of comoving radius  $X$ . Symbolically, this spatial average can be expressed as

$$\delta_Q^{\text{th}}(\tau) \equiv \frac{3}{X^3} \int_0^X dx \, x^2 \delta_Q(x, \tau), \quad (2.10)$$

where  $x \equiv |\mathbf{x}|$ , and  $\mathbf{x}$  denotes the comoving coordinates.

## 2.2. Equations of motion for the dark energy component

It remains to specify an evolution equation for the dark energy density perturbation  $\delta_Q(x, \tau)$ . We begin by writing down the continuity and Euler equations for a relativistic fluid  $\alpha$  in an expanding background in the pseudo-Newtonian approach [36],

$$\begin{aligned} \dot{\rho}_\alpha + 3\mathcal{H}(\rho_\alpha + P_\alpha) + \nabla \cdot [(\rho_\alpha + P_\alpha)\mathbf{u}_\alpha] &= 0, \\ \dot{\mathbf{u}}_\alpha + \mathcal{H}\mathbf{u}_\alpha + (\mathbf{u}_\alpha \cdot \nabla)\mathbf{u}_\alpha + \frac{\nabla P_\alpha + \mathbf{u}_\alpha \dot{P}_\alpha}{\rho_\alpha + P_\alpha} + \nabla \phi_N &= 0. \end{aligned} \quad (2.11)$$

Here,  $\nabla \equiv \partial/\partial \mathbf{x}$ ,  $\mathbf{u}_\alpha$  is the peculiar velocity of the fluid, and the potential  $\phi_N$  can be obtained from the Poisson equation

$$\nabla^2 \phi = 4\pi G a^2 \sum_\alpha \delta \rho_\alpha + 3\delta P_\alpha. \quad (2.12)$$

These equations should apply if we restrict our considerations to (i) length scales much smaller than the Hubble length, (ii) nonrelativistic peculiar velocities, and (iii) nonrelativistic sound speeds  $c_s \ll 1$ . We demonstrate in Appendix A that, at the linear level, these equations are indeed consistent with the Newtonian limit of a general relativistic formulation (see, e.g., [37–39]).

Defining the equation of state parameter for the dark energy component

$$w \equiv \frac{\bar{P}_Q}{\bar{\rho}_Q}, \quad (2.13)$$

and using the definitions  $P_\alpha \equiv \bar{P}_\alpha + \delta P_\alpha$  and  $\delta_\alpha^P \equiv \bar{\rho}_\alpha^{-1} \delta P_\alpha$ , equation (2.11) can be rewritten for  $\alpha = Q$  as

$$\begin{aligned} \dot{\delta}_Q + 3\mathcal{H}(\delta_Q^P - w\delta_Q) + \nabla \cdot [(\rho_Q + P_Q)\mathbf{u}_Q/\bar{\rho}_Q] &= 0, \\ \dot{\mathbf{u}}_Q + \mathcal{H}\mathbf{u}_Q + (\mathbf{u}_Q \cdot \nabla)\mathbf{u}_Q + \frac{\nabla \delta_Q^P + \mathbf{u}_Q(w\dot{\bar{\rho}}_Q/\bar{\rho}_Q + \dot{\delta}_Q^P)}{1 + w + \delta_Q + \delta_Q^P} + \nabla \phi_N &= 0. \end{aligned} \quad (2.14)$$

Since in our set-up the universe contains only dark matter and dark energy, the Poisson equation (2.12) now reads

$$\nabla^2 \phi = 4\pi G a^2 [\bar{\rho}_m \delta_m + \bar{\rho}_Q (\delta_Q + 3\delta_Q^P)], \quad (2.15)$$

where, for our particular problem, the dark matter density perturbation  $\delta_m(x, \tau)$  takes the form

$$\delta_m(x, \tau) = \begin{cases} \delta_m^{\text{th}}(\tau), & x \leq X(\tau), \\ 0, & x > X(\tau). \end{cases} \quad (2.16)$$

with the top hat density contrast  $\delta_m^{\text{th}}(\tau)$  given by equation (2.7).

The continuity and Euler equations (2.14) are nonlinear in the quantities  $\delta_Q$  and  $\mathbf{u}_Q$ , which even under the assumption of spherical symmetry are nontrivial to solve. Therefore, as a first approximation, we linearise them to obtain

$$\begin{aligned} \dot{\delta}_Q^{\text{lin}} + 3\mathcal{H}(\delta_Q^{P,\text{lin}} - w\delta_Q^{\text{lin}}) + (1+w)\theta_Q^{\text{lin}} &= 0, \\ \dot{\theta}_Q^{\text{lin}} + (1-3w)\mathcal{H}\theta_Q^{\text{lin}} + \frac{\nabla^2 \delta_Q^{P,\text{lin}}}{1+w} + \nabla^2 \phi_N &= 0, \end{aligned} \quad (2.17)$$

where we have defined the divergence of the dark energy velocity field to be  $\theta_Q \equiv \nabla \cdot \mathbf{u}_Q$ , and assumed  $w$  to be constant in time. Linearisation assumes that the perturbed quantities  $\delta_Q$  and  $\theta_Q$  are small. This is likely a good assumption since (i) the presence of a finite sound speed  $c_s$  naturally hinders the clustering of dark energy, keeping  $\delta_Q \simeq \delta_Q^{\text{lin}}$  small relative to  $\delta_m$ , and (ii) even in the limit  $c_s = 0$  where the clustering of dark energy is most efficient, a fully linear analysis shows that  $\delta_Q^{\text{lin}}$  is suppressed relative to  $\delta_m^{\text{lin}}$  because of the dark energy's negative equation of state parameter (see section 3). Either way, the assumption of linearity in dark energy clustering can be easily checked *a posteriori* against solutions of the evolution equations for consistency. Finally, let us stress again that we are linearising *only* the dark energy equations of motion; the evolution of the dark matter component is still fully nonlinear, and described by the spherical collapse detailed in the previous section. We shall call this the “quasi-nonlinear” approach.

Upon linearisation, it is useful to recast the equations of motion in Fourier space. Define the Fourier transform for some field  $A(x, \tau)$  as

$$\begin{aligned} A(x, \tau) &= \frac{1}{(2\pi)^3} \int d^3k \tilde{A}(k, \tau) \exp(i\mathbf{k} \cdot \mathbf{x}) \\ &= \frac{1}{2\pi^2} \int dk k^2 \tilde{A}(k, \tau) \frac{\sin(kx)}{kx}. \end{aligned} \quad (2.18)$$

Then, using the Poisson equation (2.15) and the relation  $\tilde{\delta}_Q^{P,\text{lin}} = c_s^2 \tilde{\delta}_Q^{\text{lin}} + 3\mathcal{H}(1+w)(c_s^2 - w)\tilde{\theta}_Q^{\text{lin}}/k^2$  [6], equation (2.17) can be equivalently expressed as

$$\begin{aligned} \dot{\tilde{\delta}}_Q^{\text{lin}} + 3(c_s^2 - w)\mathcal{H}\tilde{\delta}_Q^{\text{lin}} + (1+w)\tilde{\theta}_Q^{\text{lin}} &= 0, \\ \dot{\tilde{\theta}}_Q^{\text{lin}} + (1-3c_s^2)\mathcal{H}\tilde{\theta}_Q^{\text{lin}} - \frac{k^2 c_s^2}{1+w} \tilde{\delta}_Q^{\text{lin}} + 4\pi G a^2 [\bar{\rho}_m \tilde{\delta}_m + \bar{\rho}_Q (1+3c_s^2) \tilde{\delta}_Q^{\text{lin}}] &= 0, \end{aligned} \quad (2.19)$$

where we have dropped subdominant terms proportional to  $\mathcal{H}^2/k^2$ , since we are interested only in subhorizon scales  $k \gg \mathcal{H}$ . For the dark matter density contrast

$\delta_m(x, \tau)$  given in equation (2.16), the Fourier space equivalent is

$$\begin{aligned}\tilde{\delta}_m(k, \tau) &= 4\pi \int_0^{X(t)} dx \, x^2 \, \delta_m^{\text{th}}(\tau) \frac{\sin(kx)}{kx} \\ &= \delta_m^{\text{th}}(\tau) \frac{4\pi}{3} X^3 W(kX) = \frac{4\pi}{3} [(1 + \delta_{m,i}^{\text{th}}) X_i^3 - X^3] W(kX),\end{aligned}\quad (2.20)$$

where

$$W(kX) = \frac{3}{(kX)^3} [\sin(kX) - kX \cos(kX)] \quad (2.21)$$

by convention.

Lastly, we would like to relate  $\tilde{\delta}_Q^{\text{lin}}(k, \tau)$  to the average dark energy density contrast inside the top hat,  $\delta_Q^{\text{th}}(\tau)$ , as defined in equation (2.10), since this is the quantity that ultimately governs the evolution of the top hat radius  $X$  via equation (2.5). This step is simple: we only need to identify  $\delta_Q(x, \tau)$  with  $\delta_Q^{\text{lin}}(x, \tau)$ , the latter of which is obtained by Fourier transforming  $\tilde{\delta}_Q^{\text{lin}}(k, \tau)$ . Thus, equation (2.10) simplifies to

$$\delta_Q^{\text{th}}(\tau) = \frac{1}{2\pi^2} \int dk \, k^2 W(kX) \tilde{\delta}_Q^{\text{lin}}(k, \tau). \quad (2.22)$$

Our set of equations of motion is now complete.

### 3. Linear theory

Before we present the results of the spherical collapse model, let us first consider the evolution of dark matter and dark energy perturbations in the linear regime, i.e., where the dark matter perturbations are also tracked with linearised equations of motion. This exercise is useful for two reasons. Firstly, as we shall see, an understanding of the linear evolution can shed light on many essential features of the dependence of dark energy clustering on its equation of state parameter  $w$  and sound speed  $c_s$ . At the same time, the linear solution also sets the initial conditions for the spherical collapse model.

Secondly, some semi-analytic theories of structure formation such as the Press–Schechter formalism [40] and the excursion set theory [41–44] require as an input a linear critical density contrast  $\delta_{\text{coll}}^{\text{lin}}$ . In these theories a collapsed structure is assumed to have formed once the linearly evolved matter density contrast reaches the threshold value  $\delta_{\text{coll}}^{\text{lin}}$  at some time  $\tau_{\text{coll}}$ . The value of  $\delta_{\text{coll}}^{\text{lin}}$  can be determined from the spherical collapse model by interpreting  $\tau_{\text{coll}}$  as the instant at which the top hat radius vanishes. In practice, this means that in order to extract  $\delta_{\text{coll}}^{\text{lin}}$  for a particular cosmological model, we need to solve *both* the nonlinear and the linear equations of motion at the same time.

We have already written down the linearised equations of motion for the dark energy perturbations in equations (2.17) and (2.19). For the dark matter component, the corresponding equations are

$$\begin{aligned}\dot{\delta}_m^{\text{lin}} + \theta_m^{\text{lin}} &= 0, \\ \dot{\theta}_m^{\text{lin}} + \mathcal{H}\theta_m^{\text{lin}} + 4\pi G a^2 [\bar{\rho}_m \delta_m^{\text{lin}} + \bar{\rho}_Q (1 + 3c_s^2) \delta_Q^{\text{lin}}] &= 0.\end{aligned}\quad (3.1)$$

These and equation (2.19) are solved simultaneously to determine the evolution of  $\delta_Q^{\text{lin}}$  and  $\delta_m^{\text{lin}}$ .



### 3.1. Dark energy evolution in the linear regime

Let us consider first the linear evolution of the dark energy perturbations. Here, it is convenient to combine the first order differential equations (2.19) for  $\tilde{\delta}_Q^{\text{lin}}$  and  $\tilde{\theta}_Q^{\text{lin}}$  into one second order differential equation for  $\tilde{\delta}_Q^{\text{lin}}$ , and also adopt a new time variable  $s \equiv \ln a$ . Assuming  $w$  and  $c_s$  to be constant in time, we find

$$\tilde{\delta}_Q^{\text{lin}''} + \mathcal{D}(s)\tilde{\delta}_Q^{\text{lin}'} + \left[ \frac{k^2 c_s^2}{\mathcal{H}^2} \mathcal{X}(s) - \kappa(s) \right] \tilde{\delta}_Q^{\text{lin}} = \frac{3}{2}(1+w)\Omega_m(s)\tilde{\delta}_m^{\text{lin}}, \quad (3.2)$$

where  $' \equiv \partial/\partial s$ , and

$$\begin{aligned} \mathcal{D}(s) &\equiv 1 + \frac{\mathcal{H}'}{\mathcal{H}} - 3w, \\ \kappa(s) &\equiv 3w \left( 1 + \frac{\mathcal{H}'}{\mathcal{H}} \right) + \frac{3}{2}(1+w)\Omega_Q(s), \\ \mathcal{X}(s) &\equiv 1 + 3\frac{\mathcal{H}^2}{k^2} \left[ 1 + \frac{\mathcal{H}'}{\mathcal{H}} - 3(c_s^2 - w) - \frac{3}{2}(1+w)\Omega_Q(s) \right]. \end{aligned} \quad (3.3)$$

For the cosmological models considered in this work,  $\mathcal{D}(s)$  and  $|\kappa(s)|$  are of order unity, while  $\mathcal{X}(s) \approx 1$  always holds true because of our assumption of  $k \gg \mathcal{H}$ .

Equation (3.2) describes a damped harmonic oscillator with a driving force sourced by perturbations in the dark matter fluid. Exact analytic solutions do not exist for arbitrary cosmologies. However, approximate solutions can be constructed in certain limits:

- (i) *Clustering limit.* This is the limit in which  $k^2 c_s^2 / \mathcal{H}^2 \ll |\kappa| \sim 1$ . In this case, all coefficients in the differential equation are of order unity. It is therefore necessary to specify the exact time dependence of  $\mathcal{D}(s)$ ,  $\kappa(s)$  as well as  $\tilde{\delta}_m^{\text{lin}}$  in order to find a solution. Formally setting  $k = 0$ , the solution is particularly simple during the matter domination epoch, where  $\Omega_m(s) \simeq 1$ ,  $\Omega_Q(s) \ll 1$ ,  $\mathcal{H}'/\mathcal{H} \simeq -1/2$ ,  $\tilde{\delta}_m^{\text{lin}} \propto a$  and  $\tilde{\theta}_m^{\text{lin}} \simeq -\mathcal{H}\tilde{\delta}_m^{\text{lin}}$ . At  $s - s_i \gg 1$  it has the asymptotic form

$$\begin{aligned} \tilde{\delta}_Q^{\text{lin}} &\simeq \frac{1+w}{1-3w} \tilde{\delta}_m^{\text{lin}}, \\ \tilde{\theta}_Q^{\text{lin}} &\simeq -\frac{\mathcal{H}}{1+w} [3(c_s^2 - w) + 1] \tilde{\delta}_Q^{\text{lin}}, \end{aligned} \quad (3.4)$$

where we have obtained the solution for  $\tilde{\theta}_Q^{\text{lin}}$  from the continuity equation by first differentiating  $\tilde{\delta}_Q^{\text{lin}}$  with respect to time.

At first glance, the solution (3.4) for  $\tilde{\delta}_Q^{\text{lin}}$  appears to be at odds with the solution obtained in, e.g., reference [39] in the same limit (i.e.,  $\mathcal{H} \ll k \ll \mathcal{H}_s$ , where  $\mathcal{H}_s \equiv \mathcal{H}/c_s$  is the inverse of the sound horizon, or the “Jeans wavenumber”  $k_J$  as we define in equation (3.5) below). In particular, the solution of [39] depends explicitly on the sound speed  $c_s^2$ , whereas our solution does not. Part of the discrepancy can be traced to the term  $\mathcal{X}(s)$  defined in equation (3.3). In our analysis we always approximate this term as  $\mathcal{X}(s) = 1$ , while some contributions proportional to  $\mathcal{H}^2/k^2$  have been retained in the analysis of [39].



However, we believe that this discrepancy is of little consequence. As we demonstrate in Appendix B, the  $\mathcal{H} \ll k \ll \mathcal{H}_s$  limit is well-defined only for those dark energy sound speeds satisfying  $c_s^2 \lesssim 10^{-3}$ . Thus, from a numerical point of view, our approximate solution and that of [39], *where they are actually applicable*, are consistent with one another to better than one part in a thousand.

- (ii) *Non-clustering limit.* This limit corresponds to  $k^2 c_s^2 / \mathcal{H}^2 \gg |\kappa| \sim 1$ , which is also the steady-state limit ( $|\tilde{\delta}_Q^{\text{lin}''} / \tilde{\delta}_Q^{\text{lin}}|, |\tilde{\delta}_Q^{\text{lin}'} / \tilde{\delta}_Q^{\text{lin}}| \ll 1$ ). The solution can be obtained by formally setting  $\tilde{\delta}_Q^{\text{lin}''} = \tilde{\delta}_Q^{\text{lin}'} = \kappa = 0$ . Defining the “Jeans wavenumber”

$$k_J \equiv \frac{\mathcal{H}}{c_s}, \quad (3.5)$$

the steady-state/non-clustering solution then reads

$$\begin{aligned} \tilde{\delta}_Q^{\text{lin}} &\simeq \frac{3}{2}(1+w) \Omega_m(s) \left(\frac{k_J}{k}\right)^2 \tilde{\delta}_m^{\text{lin}}, \\ \tilde{\theta}_Q^{\text{lin}} &\simeq -\frac{3\mathcal{H}}{1+w} [c_s^2 - w\Omega_m(s)] \tilde{\delta}_Q^{\text{lin}}. \end{aligned} \quad (3.6)$$

Note that, unlike the clustering solution (3.4), the non-clustering solution is not restricted to the matter domination epoch. Furthermore, the derivation of (3.6) does not in fact require the assumption of a linear  $\tilde{\delta}_m$ , since  $\tilde{\delta}_m$  enters into the differential equation (3.2) only through the gravitational potential  $\phi$ , and hence the Poisson equation, which is in any case linear in  $\tilde{\delta}_m$ . This means that the steady-state/non-clustering solution (3.6) would have been equally valid had we replaced  $\tilde{\delta}_Q^{\text{lin}}$  with the Fourier transform of the top hat density contrast  $\delta_m^{\text{th}}$ . We shall make use of this solution again later on in the analysis.

The form of the non-clustering solution is akin to those commonly found in hot or warm dark matter scenarios, in which  $k_J$  is associated with the free-streaming scale of the problem (see, e.g., [45]). However, since dark energy has a non-zero  $w$  while free-streaming dark matter does not, an extra prefactor  $(1+w)$  is incurred in the solution (3.6).

- (iii) *Unstable limit.* So far we have implicitly assumed  $c_s$  to be a real number. Let us entertain ourselves for a moment with the possibility of an imaginary dark energy sound speed. In the limit  $|k^2 c_s^2 / \mathcal{H}^2| \ll 1$ , the dark energy perturbations are described by the same clustering solution as equation (3.4). Contrastingly, the  $|k^2 c_s^2 / \mathcal{H}^2| \gg 1$  limit is unstable. Formally setting  $\mathcal{D} = \kappa = \tilde{\delta}_m^{\text{lin}} = 0$ , equation (3.2) is solved in the matter domination epoch by  $\tilde{\delta}_Q^{\text{lin}} = C_1 I_0(\omega\sqrt{a}) + C_2 K_0(\omega\sqrt{a})$ , where  $I_0(x)$  and  $K_0(x)$  are the zeroth order modified Bessel functions of the first and the second kind respectively, and  $\omega \equiv 2k|c_s|/\sqrt{H_0^2 \Omega_m}$ . For  $x \equiv \omega\sqrt{a} \gg 1$ , the modified Bessel functions have the asymptotic forms  $I_0(x) \simeq \exp(x)/\sqrt{2\pi x}$  and  $K_0(x) \simeq \sqrt{\pi/2x} \exp(-x)$ . Thus, we find for the linear dark energy density contrast the asymptotic solution

$$\tilde{\delta}_Q^{\text{lin}} \sim a^{-1/4} \exp(\omega\sqrt{a}). \quad (3.7)$$

This exponential growth of  $\tilde{\delta}_Q^{\text{lin}}$  in turn sources the evolution of the dark matter density contrast via the Poisson equation (2.15). Consequently,  $\tilde{\delta}_m^{\text{lin}}$  also exhibits a similarly explosive and strongly scale-dependent growth that at first glance appears to be in conflict with our current understanding of large-scale structure formation unless  $|c_s|$  is very small. We shall therefore not pursue the case of an imaginary dark energy sound speed any further in the present work.

Given the limiting solutions (3.4) and (3.6), we can try to interpolate between the clustering and non-clustering regimes using the following (rough) interpolation formulae:

$$\begin{aligned}\tilde{\delta}_Q^{\text{lin}} &= \frac{1+w}{1-3w+(2/3)(k/k_J)^2} \tilde{\delta}_m^{\text{lin}}, \\ \tilde{\theta}_Q^{\text{lin}} &= -\frac{\mathcal{H}}{1+w} \left[ 3(c_s^2 - w) + \frac{1-3w}{1-3w+(2/3)(k/k_J)^2} \right] \tilde{\delta}_Q^{\text{lin}}.\end{aligned}\quad (3.8)$$

The maximum error is 30% at  $k \sim k_J$ . These interpolation formulae are valid during the matter domination regime, and can be used to set the initial conditions for the dark energy component in the spherical collapse model.<sup>§</sup>

Lastly, let us define a “Jeans mass” scale analogous to the Jeans wavenumber  $k_J$  given in (3.5), i.e., the mass scale at which we expect the effects of the dark energy sound speed to set in. The Jeans mass is defined here as

$$M_J(a) \equiv \frac{4\pi}{3} \bar{\rho}_m(a) \left( \frac{\lambda_J(a)}{2} \right)^3, \quad (3.9)$$

where  $\lambda_J \equiv 2\pi/k_J$ . Evaluating the expression at  $a = 1$ , we find

$$M_J = 9.7 \times 10^{23} \Omega_m c_s^3 h^{-1} M_\odot. \quad (3.10)$$

For example, given  $\Omega_m = 0.3$  and  $h = 0.7$ , we have  $M_J = 1.3 \times 10^{16} M_\odot$  for  $c_s^2 = 10^{-5}$ , and  $M_J = 4 \times 10^{14} M_\odot$  for  $c_s^2 = 10^{-6}$  today. Note that the mass here refers to the mass of the dark matter component, not the dark energy!

### 3.2. Linear threshold density

Our second motivation for considering linear theory is the computation of the linear threshold density, defined as

$$\delta_{\text{coll}}^{\text{lin}} \equiv \delta_m^{\text{th,lin}}(\tau_{\text{coll}}), \quad (3.11)$$

where  $\delta_m^{\text{th,lin}}(\tau)$  is the linearly evolved top hat matter density, and  $\tau_{\text{coll}}$  is the instant at which the top hat radius goes to zero. As the name implies,  $\delta_m^{\text{th,lin}}(\tau)$  is the linear version of the quantity  $\delta_m^{\text{th}}(\tau)$  defined in equation (2.16), and is tracked by the equations

<sup>§</sup> The full equation (3.2) in fact has an exact analytic solution encompassing all three limits discussed above in terms of Bessel functions in the matter domination epoch. However, the complexity of the solution rather obscures the simple physics behind the problem. We therefore do not quote it here.

of motion (3.1) upon the replacements

$$\begin{aligned}\delta_m^{\text{lin}}(x, \tau) &\rightarrow \delta_m^{\text{th,lin}}(\tau), \\ \theta_m^{\text{lin}}(x, \tau) &\rightarrow \theta_m^{\text{th,lin}}(\tau), \\ \delta_Q^{\text{lin}}(x, \tau) &\rightarrow \delta_Q^{\text{th,lin}}(\tau),\end{aligned}\tag{3.12}$$

where

$$\delta_Q^{\text{th,lin}}(\tau) = \frac{1}{2\pi^2} \int dk \, k^2 W(kX) \tilde{\delta}_Q^{\text{lin}}(k, \tau)\tag{3.13}$$

is the linearly evolved dark energy density contrast averaged over the top hat volume.

#### 4. Numerical results

In this section we proceed to solve numerically the evolution equations for the spherical collapse model presented earlier in section 2. We assume a flat spatial geometry for the universe so that the dark energy fraction today is related to the dark matter fraction by  $\Omega_Q = 1 - \Omega_m$ . For the choice of the parameter  $\Omega_m$  and the present Hubble rate  $H_0$ , we use the WMAP 7-year best-fit values [46]. We consider only those cases with constant  $w$  and  $c_s$ , although our formulation is applicable also to scenarios with time-dependent dark energy parameters.

We begin the evolution at a dimensionless time coordinate of

$$t_i H_0 = 2 \times 10^{-6},\tag{4.1}$$

corresponding to an initial scale factor of

$$a_i = a_0 \left( \frac{3t_i H_0 \sqrt{\Omega_m}}{2} \right)^{2/3},\tag{4.2}$$

if we assume  $t_i$  to lie well within the matter domination epoch. Taking an initial matter overdensity of  $\delta_{m,i}^{\text{th}}$  the initial value of the top hat radius can then be obtained directly from equation (2.2) given some mass  $M$ . This mass, which we dub the “halo mass”, is also the mass of dark matter contained in the final collapsed object.¶ Unless otherwise stated, the initial matter density contrast is taken to be

$$\delta_{m,i}^{\text{th}} = 3 \times 10^{-4}.\tag{4.3}$$

We have chosen the above values for the initial time and matter density contrast so that the collapse occurs at a time when the dark energy component constitutes a significant part of the universe’s energy budget.

Since the top hat evolution equation is a second order differential equation, we must also specify the time derivative of  $R$ . This can be constructed by differentiating

¶ The numerical code is written in C++ and employs GNU scientific libraries for solving the evolution equations and for interpolating the integral in equation (2.22). A verification of the convergence of equation (2.22) against the number and spacing of  $k$ -bins has been conducted.

¶ Note that the mass  $M$  here refers to the mass of the dark matter component only, although as suggested in [31], the true mass of the bound object should in principle include the contribution from the clustered dark energy component as well.

equation (2.7) with respect to time. Because the initial matter density contrast is much less than unity, we can approximate  $d\delta_m^{\text{th}}/dt \simeq d\delta_m^{\text{th,lin}}/dt \simeq H\delta_m^{\text{th,lin}}$  using linear perturbation theory, and thus,

$$\left. \frac{1}{R} \frac{dR}{dt} \right|_{t_i} \simeq \frac{2}{3t_i} \left( 1 - \frac{1}{3} \delta_{m,i}^{\text{th}} \right). \quad (4.4)$$

Finally the initial conditions for the dark energy evolution is given in section 3.1, particularly by the interpolation formula (3.8).

#### 4.1. The collapse

Figures 1 to 4 shows the physical top hat radius normalised to the initial radius as a function of the dimensionless time coordinate  $tH_0$  for several choices of  $w$ ,  $c_s$  and halo masses  $M$ . The corresponding matter overdensity (2.7) and the dark energy overdensity (2.22) are also shown in juxtaposition.

In figure 1 we present the results for a dark energy component with  $c_s^2 = 10^{-1}$  and a halo mass of  $M = 10^{14} M_\odot$  for various equation of state parameters. These choices of  $c_s$  and  $M$  satisfy  $M \ll M_J$  according to equation (3.10), and ensure that we are in the non-clustering regime. Since dark energy clustering is minimal ( $< 10^{-5}$  relative to the dark matter density contrast), only the equation of state parameter  $w$ , i.e., the homogeneous part of the dark energy fluid, plays a role in the dynamics of the spherical collapse. Indeed, as we see in the figure, the less negative the equation of state parameter, the later the collapse. The reason is that for the same  $\Omega_Q$ , the less negative  $w$  is, the earlier the dark energy comes to dominate the energy content of the universe, thereby inhibiting the growth of the top hat overdensity through Hubble expansion from an earlier stage. Comparing the  $\Lambda$ CDM case and a model with  $w = -0.7$ , the collapse time is delayed by some 20%. For equation of state parameters more negative than  $-1$ , the opposite trend is seen; in the case of  $w = -1.3$  the collapse occurs some 10% faster than in the  $\Lambda$ CDM limit.

In figure 2 we fix  $M = 10^{16} M_\odot$ , but vary the dark energy sound speed and equation of state. We choose  $w = -0.7$  and  $w = -0.8$ , since, based on results from linear theory (see section 3), dark energy clustering is most enhanced by a deviation of  $w$  from  $-1$  in the positive direction. Although the effect of dark energy clustering on the spherical collapse is quite small, the trend is clear: the smaller the sound speed, the faster the collapse. This is to be expected, since the smaller the sound speed is, the more efficiently the dark energy component clusters, and this clustering in turn contributes to sourcing the collapse of the top hat on the r.h.s. of equation (2.5). Note that although the dark energy component exhibits some degree of clustering in these cases, the density contrast for almost the entire collapse history is quite small until the last moments when  $R \rightarrow 0$ . This indicates that our quasi-nonlinear approach—in which the dark energy component is evolved with linearised equations—is valid for the model parameters adopted in this figure.

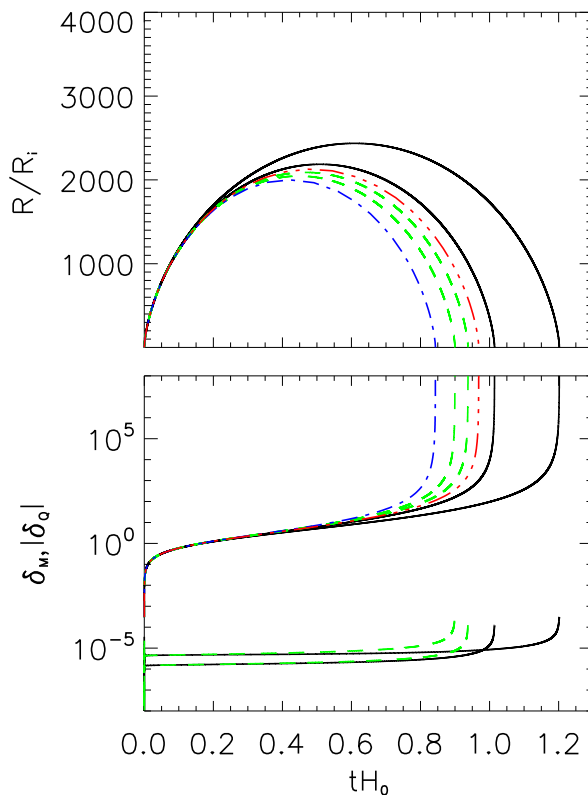


**Figure 1.** *Top:* Spherical top hat radius  $R$  normalised to the initial radius  $R_i$  as a function of the dimensionless time coordinate  $tH_0$ . The reference EdS and  $\Lambda$ CDM models are represented by the blue dot-dash and the red dot-dot-dot-dash lines respectively. The two black solid lines denote, from right to left, the cases of  $w = -0.7, -0.9$ , while the two green dashed lines denote, from right to left, the cases of  $w = -1.1, -1.3$ . For these four cases, we have chosen the dark energy sound speed to be  $c_s^2 = 10^{-1}$ , and a halo mass of  $M = 10^{14} M_\odot$ . *Bottom:* The corresponding top hat matter and dark energy density contrasts. For the cases of  $w = -1.1, -1.3$ , the dark energy density contrasts are negative, i.e., they are underdensities, and the  $\delta_Q$  values presented in this plot are absolute values. Note that in the reference EdS and  $\Lambda$ CDM models, there is no dark energy clustering. For all cases the initial matter overdensity has been chosen to be  $\delta_{m,i}^{\text{th}} = 3 \times 10^{-4}$ .

Figure 3 shows the cases of a fixed sound speed  $c_s^2 = 10^{-4}$ , equation of state parameters  $w = -0.7, -0.8$ , and three different halo masses. Figure 4 is similar, but with the sound speed fixed at  $c_s^2 = 10^{-6}$ . For these sound speeds, the corresponding Jeans masses  $M_J$  are  $4 \times 10^{17} M_\odot$  and  $4 \times 10^{14} M_\odot$  respectively. In both figures, we see that the larger the halo mass, the faster the collapse. This can be understood from the non-clustering solution (3.6) (valid here since (almost) all halo masses considered are less than the Jeans mass). Since the dominant Fourier mode is that corresponding to the comoving top hat radius  $X$  which is itself associated with the halo mass  $M$ , a reasonable generalisation of the non-clustering solution (3.6) for the dark energy component in

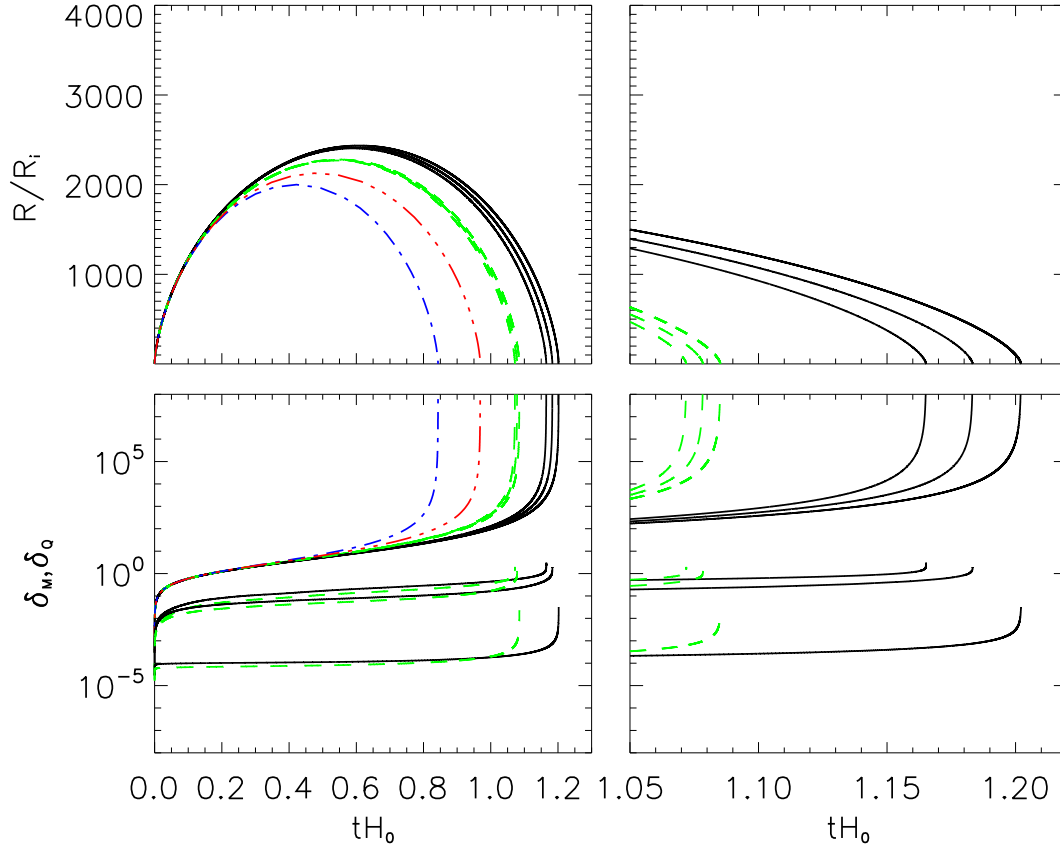


**Figure 2.** Same as figure 1, but for a fixed halo mass  $M = 10^{16} M_\odot$ . The black solid lines indicate  $w = -0.7$  and, from right to left, a dark energy sound speed of  $c_s^2 = 10^{-1}, 10^{-4}, 10^{-6}$ . The green dashed lines denote  $w = -0.8$  for the same set of dark energy sound speeds. The reference EdS and  $\Lambda$ CDM models are again represented by, respectively, the blue dot-dash and the red dot-dot-dot-dash lines. The right panels show the same results, but zoomed in on the time interval  $tH_0 = 1.05 \rightarrow 1.25$ .

terms of the halo mass would be

$$\delta_Q^{\text{th}}(\tau) \sim \frac{3}{2}(1+w)\Omega_m(\tau) \left(\frac{M}{M_J}\right)^{2/3} \delta_m^{\text{th}}(\tau). \quad (4.5)$$

The expression clearly shows that for a given sound speed, the absolute value of the dark energy density contrast increases with halo mass  $M$ . The enhanced dark energy density contrast in turn hastens the collapse of the dark matter top hat.

Note that for the case of  $M = 10^{16} M_\odot$  and  $c_s^2 = 10^{-6}$ , the dark energy density contrast is of order 0.1 for much of the collapse history. This suggests that our approximation scheme for the dark energy evolution is approaching its limits of validity; the approximation breaks down for larger masses. Thus the rule of thumb regarding the quasi-nonlinear approach appears to be that it can be safely used for halo masses up to roughly the Jeans mass  $M_J$ , but not beyond.<sup>+</sup>

<sup>+</sup> Obviously, we came to this conclusion based on the rather extreme cases of  $w = -0.7$  and  $w = -0.8$ . In general, however, we expect the validity of the quasi-nonlinear approximation scheme to be dependent also on the choice of  $w$ , where the less  $w$  deviates from  $-1$ , the higher the halo mass for which the

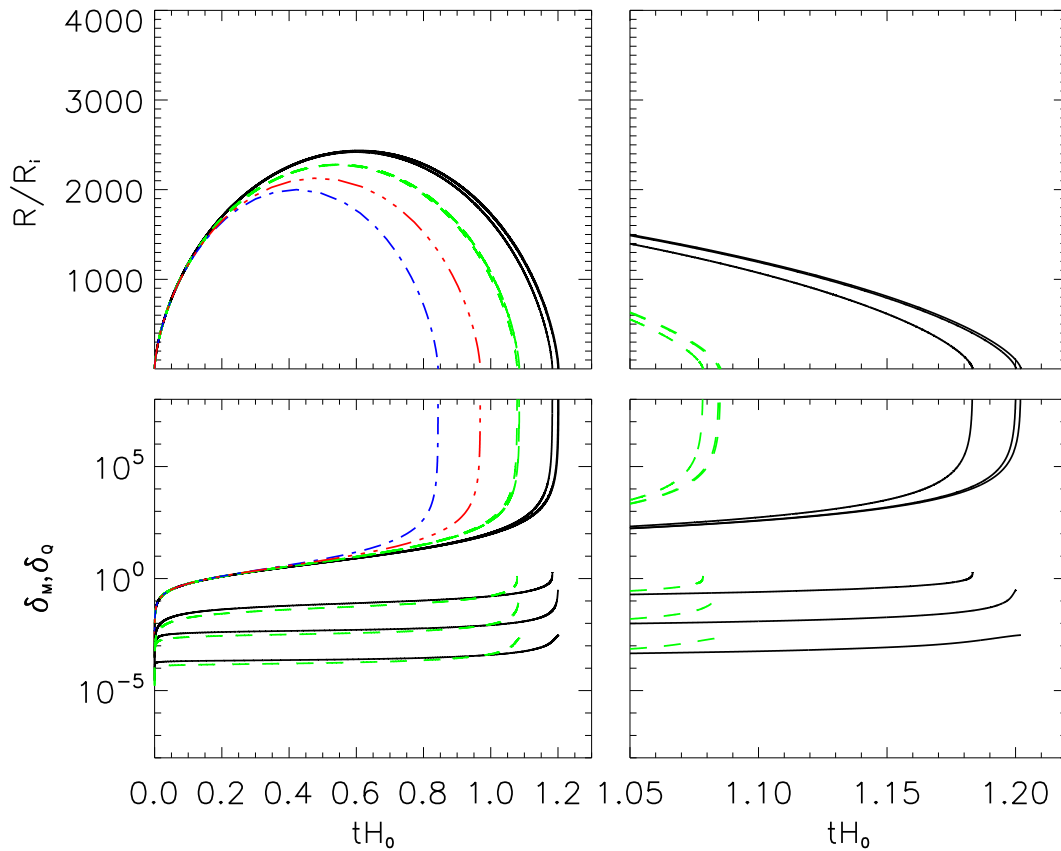


**Figure 3.** Same as figure 2, but for a fixed sound speed  $c_s^2 = 10^{-4}$ . The black solid lines denote  $w = -0.7$  and, from right to left, halo masses of  $M = 10^{12}, 10^{14}, 10^{16} M_\odot$ . The green dashed lines denote  $w = -0.8$  for the same set of halo masses. The blue dot-dash and the red dot-dot-dot-dash lines represent the reference EdS and  $\Lambda$ CDM models respectively. The right panels show the same results in the time interval between  $tH_0 = 1.05$  and  $tH_0 = 1.25$ .

#### 4.2. Linear threshold density

Next, we compute the linear critical density contrast  $\delta_{\text{coll}}^{\text{lin}}$  required for use with such semi-analytic theories as the Press–Schechter formalism and the excursion set theory. This can be achieved by solving simultaneously *both* the nonlinear and the linear equations of motion for the spherical collapse, and formally identifying  $\delta_{\text{coll}}^{\text{lin}}$  as the linearly evolved matter density contrast at the instant the top hat radius vanishes. Figure 5 shows  $\delta_{\text{coll}}^{\text{lin}}$  as a function of the halo mass for various combinations of  $w$  and  $c_s$ . The initial matter overdensities are chosen such that all halos collapse at  $z = 0$  (top panel),  $z = 1$  (middle), and  $z = 2$  (bottom).

Clearly, for the reference cases of an EdS and a  $\Lambda$ CDM universe, the linear threshold density is independent of the halo mass. However, once a finite dark energy sound speed is introduced into the picture,  $\delta_{\text{coll}}^{\text{lin}}$  becomes mass-dependent, with  $\delta_{\text{coll}}^{\text{lin}}(M)$  a monotonically increasing function of  $M$  when  $w > -1$  and a monotonically decreasing function of  $M$  when  $w < -1$ . The approximation scheme remains applicable.



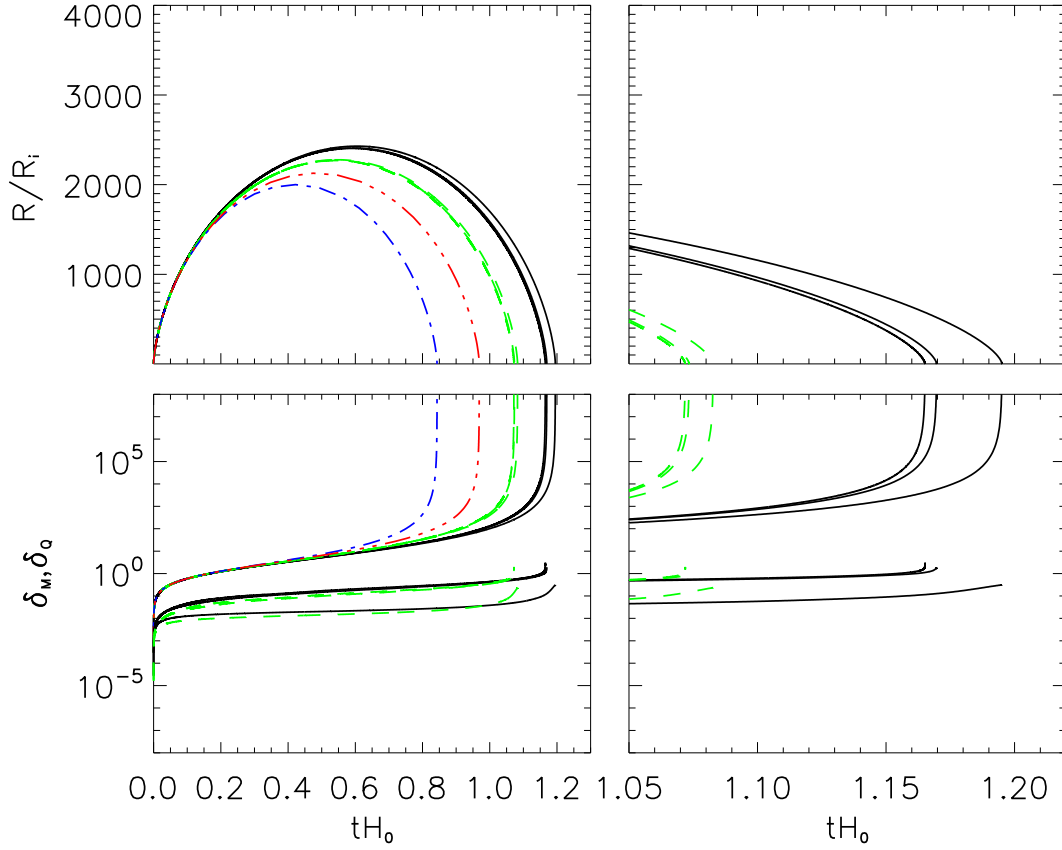


**Figure 4.** Same as figure 3, but with the sound speed fixed at  $c_s^2 = 10^{-6}$ .

function of  $M$  when  $w < -1$ . The  $M$ -dependence is however quite weak for those cases with  $w$  close to  $-1$ , since dark energy clustering is generally suppressed by a factor  $(1 + w)$ .

The most interesting case presented here is that for  $w = -0.8$ , especially for  $c_s^2 = 10^{-5}$  and  $c_s^2 = 10^{-6}$  (corresponding Jeans masses:  $1.3 \times 10^{16} M_\odot$  and  $4 \times 10^{14} M_\odot$ ). Here, we see that at  $M \ll M_J$ ,  $\delta_{\text{coll}}^{\text{lin}}$  is at its lowest value and is essentially independent of  $M$ , indicating that we are in the fully non-clustering regime. As we move to higher values of  $M$ , we encounter a transition region where  $\delta_{\text{coll}}^{\text{lin}}$  rises with  $M$ . Once  $M \gg M_J$ , however,  $\delta_{\text{coll}}^{\text{lin}}$  reaches a plateau, where clustering is most efficient and  $\delta_{\text{coll}}^{\text{lin}}$  is again independent of  $M$ . Interestingly, a similar pattern can also be seen in the  $w < -1$  cases, where the dark energy density contrasts are negative, corresponding to dark energy underdensities, which have a negative effect on the clustering of matter. This negative effect is strongest for masses larger than the Jeans mass.

The dependence of  $\delta_{\text{coll}}^{\text{lin}}$  on the collapse redshift is also quite clear in figure 5. The later the collapse, the larger the difference between the values of  $\delta_{\text{coll}}^{\text{lin}}$  for the clustering and the non-clustering solutions. The reason is simply that the contribution of dark energy to the total energy budget in the universe increases with time. This means the effect of dark energy clustering also becomes more important at lower redshifts.

Finally, we caution the reader again that our quasi-nonlinear approximation breaks

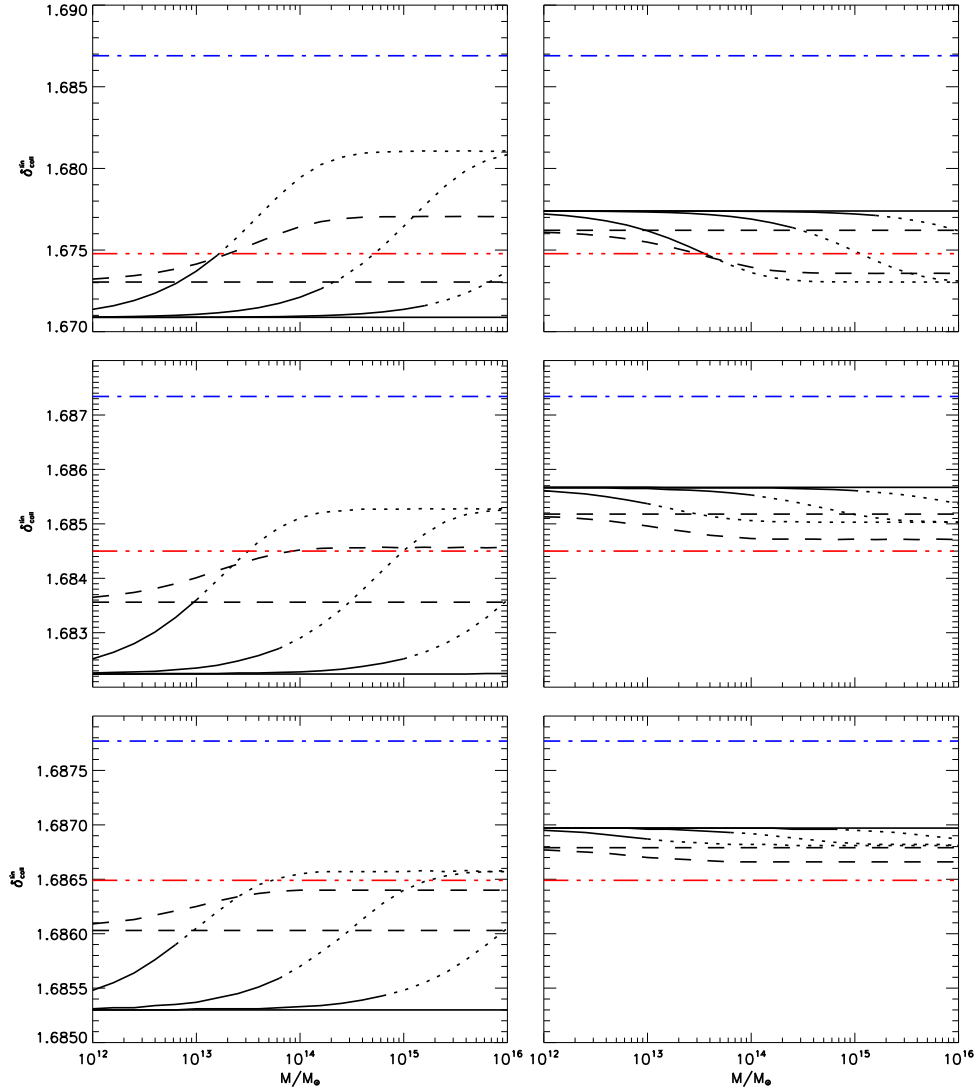


**Figure 5.** Linear threshold density  $\delta_{\text{coll}}^{\text{lin}}$  as a function of the halo mass  $M$  at various collapse redshifts. *Top left:* Collapse redshift of  $z = 0$ . Solid lines denote models with  $w = -0.8$  and, from top to bottom,  $c_s^2 = 10^{-6}, 10^{-5}, 10^{-4}, 10^{-2}$ . Dashed lines denote models with  $w = -0.9$  and  $c_s^2 = 10^{-6}, 10^{-2}$ . For those cases in which  $\delta_Q^{\text{th}} > 1$  during the collapse, we indicate the results with dotted lines. The blue dot-dash and the red dot-dot-dot-dash lines represent the reference EdS and  $\Lambda$ CDM models respectively. *Top right:* Same as top left, but with the solid lines denoting models with  $w = -1.2$  and, from top to bottom,  $c_s^2 = 10^{-2}, 10^{-4}, 10^{-5}, 10^{-6}$ . Dashed lines represent models with  $w = -1.1$  and  $c_s^2 = 10^{-2}, 10^{-6}$ . *Middle:* Same as top panel, but for a collapse redshift of  $z = 1$ . *Bottom:* Same as top panel, but for a collapse redshift of  $z = 2$ .

down if the dark energy density contrast inside the top hat becomes too large, especially when the halo mass approaches or exceeds the Jeans mass associated with a chosen sound speed. As a rule of thumb, we take the condition of breakdown to be  $\delta_Q^{\text{th}} \geq 1$  at any time during the collapse process. To alert the reader to those cases where the breakdown condition is met, we indicate the resulting linear threshold densities  $\delta_{\text{coll}}^{\text{lin}}$  in figure 5 with dotted lines; in these cases, the exact values of  $\delta_{\text{coll}}^{\text{lin}}$  are unreliable. Clearly, for equation

of state parameters that deviate significantly from  $w = -1$  (e.g.,  $w = -0.8, -1.2$ ), our approximate approach breaks down already at  $M < M_J$ . For  $w = -0.9, -1.1$ , the approach appears to remain valid for a larger mass range.

The breakdown of our approximation in the clustering limit also explains why we do not recover the exact results of reference [31] for  $c_s^2 = 0$  and  $w = -0.7, -1.3$ . In fact, in the clustering limit, our approximation appears to overestimate the effect of dark energy clustering on the linear threshold density; had we included all nonlinear effects, nonlinear dark energy clustering would feed back on the matter clustering more effectively, thereby leading to an earlier collapse for  $w > -1$  (and a later collapse for  $w < -1$ ). An earlier collapse means that the linearly evolved matter density contrast would reach a lower value at the time of collapse, so that the real  $\delta_{\text{coll}}^{\text{lin}}$  in the clustering limit would be lower than our estimate in figure 5.

#### 4.3. Virialisation

In reality the collapse of an overdense region will never take place in the way described above, since density fluctuations inside the region will moderate the infall, and the system reaches virial equilibrium before the matter density can ever become infinite. For a single component system such as the case of a dark matter-dominated EdS universe, the process of virialisation and the radius at which virial equilibrium is attained can be obtained directly from the spherical collapse physics by assuming energy conservation between the time of turnaround—defined as the moment at which the top hat radius begins to shrink—and the time at which virial equilibrium is established. The result turns out to be rather simple,

$$R_{\text{vir}} = \frac{1}{2}R_{\text{turnaround}}, \quad (4.6)$$

i.e., virialisation is complete by the time the top hat radius decreases to half its value at turnaround.

For more complicated systems, such as the two fluid system considered in this paper, the conditions of energy conservation need to be modified. The time of virialisation can still be taken to be the instant at which the virial theorem is satisfied. However, the problem is complicated by the fact that we do not know how or if the dark energy fluid takes part in the virialisation process (see, e.g., [47, 48]). Therefore, for simplicity, we adopt equation (4.6) as the virialisation condition for this paper, and define the virial overdensity as

$$\Delta_{\text{vir}} \equiv \frac{\rho_m^{\text{th}}(\tau_{\text{vir}})}{\bar{\rho}_m(\tau_{\text{vir}})}, \quad (4.7)$$

where  $\tau_{\text{vir}}$  is the time at which  $R = R_{\text{vir}}$ . We expect the quantitative results to be somewhat sensitive to our choice of the virialisation condition, but the qualitative features should be unaffected.

Figure 6 shows  $\Delta_{\text{vir}}$  as a function of the halo mass  $M$  for various combinations of  $w$  and  $c_s^2$ . The initial top hat matter density contrast  $\delta_{m,i}^{\text{th}}$  has been fixed so that all

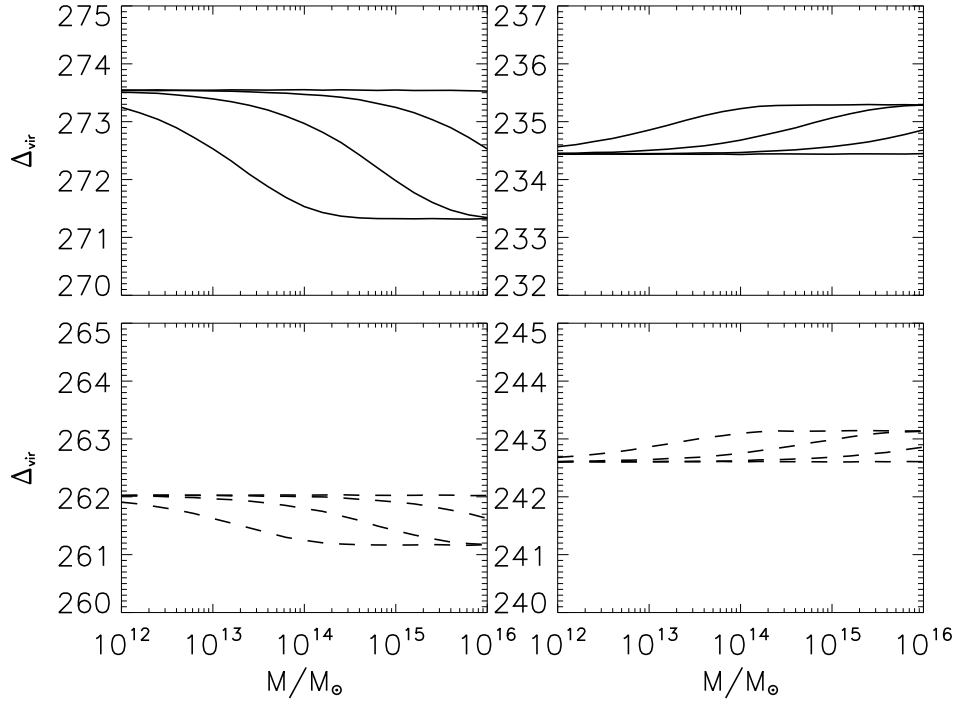


**Figure 6.** Virial overdensity  $\Delta_{\text{vir}}$  as a function of the halo mass  $M$  for different dark energy equation of state parameters and sound speeds. In all cases  $\delta_{m,i}^{\text{th}}$  has been chosen such that the collapse occurs at  $z = 0$ . *Top left:*  $w = -0.8$  and, from top to bottom,  $c_s^2 = 10^{-2}, 10^{-4}, 10^{-5}, 10^{-6}$ . *Top right:*  $w = -1.2$  and  $c_s^2 = 10^{-6}, 10^{-5}, 10^{-4}, 10^{-2}$ . *Bottom left:*  $w = -0.9$  and  $c_s^2 = 10^{-2}, 10^{-6}$ . *Bottom right:*  $w = -1.1$  and  $c_s^2 = 10^{-6}, 10^{-2}$ .

halos collapse at  $z = 0$ . As a reference point, for halos that collapse today,  $\Delta_{\text{vir}} = 147$  and  $\Delta_{\text{vir}} = 252$  for an EdS and a  $\Lambda$ CDM universe respectively (we do not plot these in figure 6 because they fall out of the plotting range).

Similar to the linear threshold density  $\delta_{\text{coll}}^{\text{lin}}$ ,  $\Delta_{\text{vir}}$  is first and foremost dependent on the choice of  $w$ . Introducing a finite dark energy sound speed into the picture induces for  $\Delta_{\text{vir}}$  a dependence on the halo mass  $M$ . However, while  $\delta_{\text{coll}}^{\text{lin}}$  increases with  $M$  for cosmologies with  $w > -1$ ,  $\Delta_{\text{vir}}$  decreases with it. The opposite trend is seen for cosmologies with  $w < -1$ . As with  $\delta_{\text{coll}}^{\text{lin}}$ , again we see an asymptotic non-clustering value for  $\Delta_{\text{vir}}$  at  $M \ll M_J$ , a transition region at  $M \sim M_J$  where  $\Delta_{\text{vir}}$  varies strongly with  $M$ , and a second asymptotic region in the  $M \gg M_J$  clustering limit.

The results in figure 6 are for a collapse redshift of  $z = 0$ . For halos that collapse earlier, the dependence of  $\Delta_{\text{vir}}$  on the halo mass is qualitatively similar to the  $z = 0$  case, but the difference in  $\Delta_{\text{vir}}$  between the clustering and the non-clustering limits is smaller. This trend is reminiscent of the results in figure 5 for the linear threshold density  $\delta_{\text{coll}}^{\text{th}}$  for different collapse redshifts.

Finally, note that some authors define the virial overdensity as the top hat density at the time of virialisation  $\tau_{\text{vir}}$ , but normalised to the background density evaluated at the *collapse time*  $\tau_{\text{coll}}$ . This means that instead of, e.g.,  $\Delta_{\text{vir}} = 147$  for the EdS model

according to our definition (4.7), one finds a higher value of 179 simply because between  $\tau_{\text{vir}}$  and  $\tau_{\text{coll}}$  the background density has become smaller due to the Hubble expansion. Since the dark energy sound speed does not play a role in the background expansion, the effect of these differing definitions is only to induce a shift in the normalisation of  $\Delta_{\text{vir}}$  for a given set of  $w$  and  $\Omega_Q$ . The  $M$ -dependence of  $\Delta_{\text{vir}}$  is unaffected.

## 5. Discussions and conclusions

While a dark energy fluid with a negative equation of state parameter appears to describe the apparent accelerated expansion of our universe with reasonable success, the precise nature and properties of this dark energy remain undetermined. In this paper, we have addressed some aspects of the dark energy’s role in cosmic structure formation. Specifically, we have considered a generic dark energy fluid parameterised by a constant equation of state parameter  $w$  and sound speed  $c_s$ , and determined their impact on the formation of gravitationally bound objects.

Our main tool is the spherical collapse model, incorporating a nonrelativistic dark matter component and a generic dark energy fluid described above. Such a model has been investigated by other authors previously in the limit where the dark energy is (i) non-clustering, i.e.,  $c_s \rightarrow \infty$ , or (ii) comoving with the dark matter, i.e.,  $c_s \rightarrow 0$ . In this work, we have generalised the spherical collapse model to describe those intermediate cases characterised by an arbitrary  $c_s$ . Although we have focussed on scenarios with constant  $w$  and  $c_s$ , our approach is equally applicable to dark energy fluids described by time-dependent parameters. Along the way, we have also provided a detailed description of dark energy evolution in the linear regime—again for arbitrary  $w$  and  $c_s$ , and identified some salient features of dark energy clustering.

The dark energy component changes the evolution of the spherical collapse through its effect on the overall expansion of the universe as well as through its own clustering abilities. In the non-clustering limit, only the equation of state parameter  $w$  plays a role in the dynamics of the spherical collapse by altering the rate of the Hubble expansion. When the dark energy is able to cluster, however, then the dark energy density contrast also sources the evolution of the dark matter density perturbations. The amount of dark energy clustering is determined by both  $w$  and  $c_s$ .

In addition, since the introduction of a dark energy sound speed  $c_s$  necessarily brings into the picture a “Jeans scale” and hence a “Jeans mass”  $M_J$ , we find that the same sound speed can influence the spherical collapse dynamics in different ways depending on the mass of the collapsed object or the “halo mass”  $M$ . This mass dependence is especially manifest when we compute the virial overdensity  $\Delta_{\text{vir}}$  and the linearly extrapolated threshold density  $\delta_{\text{coll}}^{\text{lin}}$ . In both cases, we find two asymptotic regions corresponding to the non-clustering  $M \ll M_J$  limit and the clustering  $M \gg M_J$  limit, where the value of  $\Delta_{\text{vir}}$  or  $\delta_{\text{coll}}^{\text{lin}}$  is practically constant with respect to  $M$ . In between these limits is a transition region, in which  $\Delta_{\text{vir}}$  ( $\delta_{\text{coll}}^{\text{lin}}$ ) declines (grows) strongly with  $M$ . Observing this transition region will be tell-tale sign that dark energy is dynamic, and

a great leap towards pinning down its clustering properties.

One possible way to discern this halo mass-dependent dark energy clustering is to measure the cluster mass function. Already it has been shown in, e.g., reference [31] that the difference between a clustering ( $c_s = 0$ ) and a homogeneous ( $c_s \rightarrow \infty$ ) dark energy fluid can be an order unity effect on the expected number of clusters at the high mass tail of the mass function. It remains to be seen how exactly an arbitrary dark energy sound speed would alter this conclusion, but some additional scale-dependent effects are almost guaranteed to be present.

Finally, let us remind the reader again that in our spherical collapse analysis we have simplified the equations of motion for the dark energy component so that only terms linear in the dark energy density contrast have been retained. This approach is strictly not valid for those cases in which the dark energy density contrast exceeds unity during the collapse process, and is especially prone to breakdown for cosmologies with an equation of state parameter that deviates significantly from  $w = -1$ . In these cases, a fully nonlinear analysis is required in order to compute accurately such quantities as  $\Delta_{\text{vir}}$  and  $\delta_{\text{coll}}^{\text{lin}}$  for comparison with observations. However, the qualitative features of dark energy clustering should not be affected by our simplified approach. A fully nonlinear analysis would require that we solve the equations of motion for the dark energy component—two  $(1+1)$ -dimensional partial differential equations—using either a grid-based finite difference scheme or a Lagrangian method akin to a smoothed particle hydrodynamics simulation. Investigation is already underway and we hope to report the results in a future publication.

## Acknowledgments

We thank Jacob Brandbyge, Jan Hamann and Cornelius Rampf for comments on the manuscript. Y<sup>3</sup>W thanks Guillermo Ballesteros for useful discussions. OEB acknowledges support from the Villum Foundation.

## Appendix A. From general relativity to the pseudo-Newtonian approach

We demonstrate in this section that, at linear order, the pseudo-Newtonian approach adopted in this work is indeed consistent with the Newtonian limit of a general relativistic formulation. We work in the conformal Newtonian gauge, in which the perturbed line element is given by [49]

$$ds^2 = a^2(\tau) \{ -[1 + 2\psi(\tau, \mathbf{x})]d\tau^2 + [1 - 2\phi(\tau, \mathbf{x})](dx^2 + dy^2 + dz^2) \}, \quad (\text{A.1})$$

for a flat background spatial geometry. Assuming zero anisotropic stress so that  $\psi = \phi$ , the equations of motion in Fourier space for the dark matter and dark energy components [37–39] are, respectively,

$$\begin{aligned} \dot{\delta}_m + \theta_m - 3\dot{\phi} &= 0, \\ \dot{\theta}_m + \mathcal{H}\theta_m - k^2\phi &= 0, \end{aligned} \quad (\text{A.2})$$

and

$$\begin{aligned}\dot{\delta}_Q + 3(c_s^2 - w)\mathcal{H}\delta_Q + (1 + w)D\theta_Q - 3(1 + w)\dot{\phi} &= 0, \\ \dot{\theta}_Q + (1 - 3c_s^2)\mathcal{H}\theta_Q - \frac{k^2 c_s^2}{1 + w}\delta_Q - k^2\phi &= 0,\end{aligned}\tag{A.3}$$

where  $D \equiv 1 + 9(c_s^2 - w)\mathcal{H}^2/k^2$ , and  $\dot{D} = 18(c_s^2 - w)\dot{\mathcal{H}}\mathcal{H}/k^2$ . Rearranging equations (A.2) and (A.3) respectively into second order differential equations, we find

$$\ddot{\delta}_m + \mathcal{H}\dot{\delta}_m = 3\mathcal{H}\dot{\phi} - k^2\phi + 3\ddot{\phi},\tag{A.4}$$

and

$$\begin{aligned}\ddot{\delta}_Q + [(1 - 3w)\mathcal{H} - \dot{D}/D]\dot{\delta}_Q \\ + \{Dc_s^2 k^2 + 3(c_s^2 - w)[\dot{\mathcal{H}} + (1 - 3c_s^2)\mathcal{H}^2 - (\dot{D}/D)\mathcal{H}]\}\delta_Q \\ = (1 + w)\{3[(1 - 3c_s^2)\mathcal{H} - \dot{D}/D]\dot{\phi} - Dk^2\phi + 3\ddot{\phi}\},\end{aligned}\tag{A.5}$$

assuming time-independent  $w$  and  $c_s^2$ .

In order to take the subhorizon (i.e.,  $k \gg \mathcal{H}$ ) limit of equation (A.5), we note that  $\dot{\mathcal{H}} \sim O(\mathcal{H}^2)$ . Thus, we can replace all occurrences of  $D$  with  $D = 1$  and  $\dot{D}/D$  with  $\dot{D}/D = 0$ . One last step concerns the coefficient of the  $\delta_Q$  term on the LHS: we group all contributions proportional to  $c_s^2$  together to get

$$\left\{ c_s^2 k^2 \left[ 1 + 3 \frac{\mathcal{H}^2}{k^2} \left( \frac{\dot{\mathcal{H}}}{\mathcal{H}^2} + 1 - 3(c_s^2 - w) \right) \right] - 3w(\mathcal{H}^2 + \dot{\mathcal{H}}) \right\} \delta_Q,\tag{A.6}$$

and set the  $O(\mathcal{H}^2/k^2)$  terms in [...] to zero. Thus, we find

$$\begin{aligned}\ddot{\delta}_Q + (1 - 3w)\mathcal{H}\dot{\delta}_Q + [c_s^2 k^2 - 3w(\dot{\mathcal{H}} + \mathcal{H}^2)]\delta_Q \\ = (1 + w)[3(1 - 3c_s^2)\mathcal{H}\dot{\phi} - k^2\phi + 3\ddot{\phi}]\end{aligned}\tag{A.7}$$

for the subhorizon limit of equation (A.5).

It remains to specify the metric perturbation  $\phi$  in terms of the density and velocity perturbations via the Einstein equation. Using the expressions given in, e.g., [49], we obtain

$$\begin{aligned}k^2\phi &= -\frac{3}{2}\mathcal{H}^2 \sum_{\alpha} \Omega_{\alpha} \left[ \delta_{\alpha} + 3 \frac{\mathcal{H}^2}{k^2} (1 + w_{\alpha}) \frac{\theta_{\alpha}}{\mathcal{H}} \right], \\ \mathcal{H}\dot{\phi} &= \frac{3}{2}\mathcal{H}^2 \sum_{\alpha} \Omega_{\alpha} \frac{\mathcal{H}^2}{k^2} \left[ \delta_{\alpha} + (1 + w_{\alpha}) \left( 1 + 3 \frac{\mathcal{H}^2}{k^2} \right) \frac{\theta_{\alpha}}{\mathcal{H}} \right], \\ \ddot{\phi} &= \frac{3}{2}\mathcal{H}^2 \sum_{\alpha} \Omega_{\alpha} \left\{ \left[ c_{\alpha}^2 + \frac{\mathcal{H}^2}{k^2} \left( \frac{2}{\mathcal{H}^2} \frac{\ddot{a}}{a} - 4 \right) \right] \delta_{\alpha} \right. \\ &\quad \left. + 3(1 + w_{\alpha}) \frac{\mathcal{H}^2}{k^2} \left[ c_{\alpha}^2 - w_{\alpha} - 1 + \left( \frac{2}{\mathcal{H}^2} \frac{\ddot{a}}{a} - 4 \right) \frac{\mathcal{H}^2}{k^2} \right] \frac{\theta_{\alpha}}{\mathcal{H}} \right\}.\end{aligned}\tag{A.8}$$

For the problem at hand, the summation is performed over  $\alpha = m, Q$ , and the notation should be understood to mean  $\Omega_{\alpha} = \Omega_{\alpha}(\tau)$ ,  $w_m = 0$ ,  $w_Q = w$ ,  $c_m^2 = 0$ , and  $c_Q^2 = c_s^2$ . Combining these expressions to form the RHS of equation (A.4), we find the leading order contribution in the subhorizon limit to be

$$3\mathcal{H}\dot{\phi} - k^2\phi + 3\ddot{\phi} \simeq \frac{3}{2}\mathcal{H}^2 \sum_{\alpha} \Omega_{\alpha} (1 + 3c_{\alpha}^2) \delta_{\alpha}.\tag{A.9}$$



Similarly, we find for the RHS of equation (A.5),

$$3(1 - 3c_s^2)\mathcal{H}\dot{\phi} - k^2\phi + 3\ddot{\phi} \simeq \frac{3}{2}\mathcal{H}^2 \sum_{\alpha} \Omega_{\alpha}(1 + 3c_{\alpha}^2)\delta_{\alpha}, \quad (\text{A.10})$$

again to leading order in  $\mathcal{H}/k$ . Note that RHS of equations (A.9) and (A.10) are identical as a result of a  $\mathcal{H}^2/k^2$ -suppressed  $\mathcal{H}\dot{\phi}$  term relative to the  $k^2\phi$  and  $\ddot{\phi}$  terms, as can be seen in equation (A.8). We have *not* assumed  $c_s^2 \ll 1$  to arrive at this result.

Thus, equations (A.4) and (A.5) now become, respectively,

$$\begin{aligned} \ddot{\delta}_m + \mathcal{H}\dot{\delta}_m &= \frac{3}{2}\mathcal{H}^2[\Omega_m(\tau)\delta_m + \Omega_Q(\tau)(1 + 3c_s^2)\delta_Q], \\ \ddot{\delta}_Q + (1 - 3w)\mathcal{H}\dot{\delta}_Q + [c_s^2k^2 - 3w(\mathcal{H} + \mathcal{H}^2)]\delta_Q \\ &= (1 + w)\frac{3}{2}\mathcal{H}^2[\Omega_m(\tau)\delta_m + \Omega_Q(\tau)(1 + 3c_s^2)\delta_Q]. \end{aligned} \quad (\text{A.11})$$

These equations are consistent with the outcome of the pseudo-Newtonian approach (equations (3.1) to (3.3)).

## Appendix B. Validity of the $\mathcal{H}_s^2 \gg k^2 \gg \mathcal{H}^2$ regime

A number of approximations have been made in order to arrive at the final equation of motion (A.11) for the dark energy component in the subhorizon limit. We have demanded that  $(1 - 3w)\mathcal{H} \gg \dot{D}/D$  in equation (A.5), which limits the use of the approximate equation (A.11) to  $\mathcal{H}^2/k^2 \ll 0.074 \rightarrow 0.15$ , depending on the sound speed assumed. We have also assumed  $D \approx 1$ , equivalent to imposing a limit of  $\mathcal{H}^2/k^2 \ll 0.055 \rightarrow 0.1$  on the validity of our approximate equations. In practice, we might want to choose a benchmark limit of

$$\max\left(\frac{\mathcal{H}^2}{k^2}\right) = 0.01, \quad (\text{B.1})$$

in order to keep all superhorizon contributions at a truly subdominant level.

Similarly, if we wish to take the super-sound-horizon limit (i.e., the clustering limit,  $k \ll \mathcal{H}_s$ , where  $\mathcal{H}_s \equiv \mathcal{H}/c_s$ ), then from equation (3.2) or (A.11), we see that

$$\max\left(\frac{k^2c_s^2}{\mathcal{H}^2}\right) = 0.1 \quad (\text{B.2})$$

would work as a good benchmark limit to ensure the subdominance of sub-sound-horizon contributions. The two benchmark limits (B.1) and (B.2) together define the  $\mathcal{H}_s^2 \gg k^2 \gg \mathcal{H}^2$  regime (or the “clustering regime” in this work).

From here, it is easy to see that the two limits (B.1) and (B.2) combine to set a constraint on the dark energy sound speed of

$$c_s^2 \lesssim 10^{-3} \quad (\text{B.3})$$

in the  $\mathcal{H}_s^2 \gg k^2 \gg \mathcal{H}^2$  regime. If we were to exceed this constraint, we also run the risk of increasing the superhorizon ( $\mathcal{H}^2/k^2$ ) and/or sub-sound-horizon ( $k^2c_s^2/\mathcal{H}^2$ ) contributions to any approximate analytic solution to beyond the “negligible” level, in which case the  $\mathcal{H}_s^2 \gg k^2 \gg \mathcal{H}^2$  regime becomes ill-defined.

## References

- [1] E. J. Copeland, M. Sami and S. Tsujikawa, “Dynamics of dark energy,” *Int. J. Mod. Phys. D* **15** (2006) 1753 [arXiv:hep-th/0603057].
- [2] J. A. Frieman, “Lectures On Dark Energy And Cosmic Acceleration,” *AIP Conf. Proc.* **1057** (2008) 87 [arXiv:0904.1832 [astro-ph.CO]].
- [3] R. Bean, “TASI Lectures on Cosmic Acceleration,” arXiv:1003.4468 [astro-ph.CO].
- [4] J. Weller and A. M. Lewis, “Large Scale Cosmic Microwave Background Anisotropies and Dark Energy,” *Mon. Not. Roy. Astron. Soc.* **346** (2003) 987 [arXiv:astro-ph/0307104].
- [5] S. DeDeo, R. R. Caldwell and P. J. Steinhardt, “Effects of the sound speed of quintessence on the microwave background and large scale structure,” *Phys. Rev. D* **67** (2003) 103509 [Erratum-ibid. *D* **69** (2004) 129902] [arXiv:astro-ph/0301284].
- [6] R. Bean and O. Dore, “Probing dark energy perturbations: the dark energy equation of state and speed of sound as measured by WMAP,” *Phys. Rev. D* **69** (2004) 083503 [arXiv:astro-ph/0307100].
- [7] S. Hannestad, “Constraints on the sound speed of dark energy,” *Phys. Rev. D* **71** (2005) 103519 [arXiv:astro-ph/0504017].
- [8] R. de Putter, D. Huterer and E. V. Linder, “Measuring the Speed of Dark: Detecting Dark Energy Perturbations,” *Phys. Rev. D* **81** (2010) 103513 [arXiv:1002.1311 [astro-ph.CO]].
- [9] W. Hu and R. Scranton, “Measuring Dark Energy Clustering with CMB-Galaxy Correlations,” *Phys. Rev. D* **70** (2004) 123002 [arXiv:astro-ph/0408456].
- [10] P. S. Corasaniti, T. Giannantonio and A. Melchiorri, “Constraining dark energy with cross-correlated CMB and Large Scale Structure data,” *Phys. Rev. D* **71** (2005) 123521 [arXiv:astro-ph/0504115].
- [11] T. Giannantonio, R. Scranton, R. G. Crittenden, R. C. Nichol, S. P. Boughn, A. D. Myers and G. T. Richards, “Combined analysis of the integrated Sachs-Wolfe effect and cosmological implications,” *Phys. Rev. D* **77** (2008) 123520 [arXiv:0801.4380 [astro-ph]].
- [12] H. Li and J. Q. Xia, “Constraints on Dark Energy Parameters from Correlations of CMB with LSS,” *JCAP* **1004** (2010) 026 [arXiv:1004.2774 [astro-ph.CO]].
- [13] N. N. Weinberg and M. Kamionkowski, “Constraining dark energy from the abundance of weak gravitational lenses,” *Mon. Not. Roy. Astron. Soc.* **341** (2003) 251 [arXiv:astro-ph/0210134].
- [14] M. Jarvis, B. Jain, G. Bernstein and D. Dolney, “Dark Energy Constraints from the CTIO Lensing Survey,” *Astrophys. J.* **644** (2006) 71 [arXiv:astro-ph/0502243].
- [15] C. Schimd *et al.*, “Tracking quintessence by cosmic shear: Constraints from VIRMOS-Desart and CFHTLS and future prospects,” *Astron. Astrophys.* **463** (2007) 405 [arXiv:astro-ph/0603158].
- [16] E. Sefusatti, C. Vale, K. Kadota and J. Frieman, “Primordial non-Gaussianity and dark energy constraints from cluster surveys,” *Astrophys. J.* **658** (2007) 669 [arXiv:astro-ph/0609124].
- [17] M. Takada, “Can A Galaxy Redshift Survey Measure Dark Energy Clustering?,” *Phys. Rev. D* **74** (2006) 043505 [arXiv:astro-ph/0606533].
- [18] L. R. Abramo, R. C. Batista and R. Rosenfeld, “The signature of dark energy perturbations in galaxy cluster surveys,” *JCAP* **0907** (2009) 040 [arXiv:0902.3226 [astro-ph.CO]].
- [19] J. M. Alimi, A. Fuzfa, V. Boucher, Y. Rasera, J. Courtin and P. S. Corasaniti, “Imprints of Dark Energy on Cosmic Structure Formation I) Realistic Quintessence Models,” *Mon. Not. Roy. Astron. Soc.* **401** (2010) 775 [arXiv:0903.5490 [astro-ph.CO]].
- [20] J. E. Gunn and J. R. I. Gott, “On the infall of matter into cluster of galaxies and some effects on their evolution,” *Astrophys. J.* **176** (1972) 1.
- [21] P. J. E. Peebles, “Tests of Cosmological Models Constrained by Inflation,” *Astrophys. J.* **284** (1984) 439.
- [22] S. Weinberg, “Anthropic Bound on the Cosmological Constant,” *Phys. Rev. Lett.* **59** (1987) 2607.
- [23] O. Lahav, P. B. Lilje, J. R. Primack and M. J. Rees, “Dynamical effects of the cosmological constant,” *Mon. Not. Roy. Astron. Soc.* **251** (1991) 128.

- [24] L. M. I. Wang and P. J. Steinhardt, “Cluster Abundance Constraints on Quintessence Models,” *Astrophys. J.* **508** (1998) 483 [arXiv:astro-ph/9804015].
- [25] D. F. Mota and C. van de Bruck, “On the spherical collapse model in dark energy cosmologies,” *Astron. Astrophys.* **421** (2004) 71 [arXiv:astro-ph/0401504].
- [26] C. Horellou and J. Berge, “Dark energy and the evolution of spherical overdensities,” *Mon. Not. Roy. Astron. Soc.* **360** (2005) 1393 [arXiv:astro-ph/0504465].
- [27] M. Bartelmann, M. Doran and C. Wetterich, “Non-linear Structure Formation in Cosmologies with Early Dark Energy,” *Astron. Astrophys.* **454** (2006) 27 [arXiv:astro-ph/0507257].
- [28] L. R. Abramo, R. C. Batista, L. Liberato and R. Rosenfeld, “Structure formation in the presence of dark energy perturbations,” *JCAP* **0711** (2007) 012 [arXiv:0707.2882 [astro-ph]].
- [29] S. Basilakos, J. C. Bueno Sanchez and L. Perivolaropoulos, “The spherical collapse model and cluster formation beyond the  $\Lambda$  cosmology: Indications for a clustered dark energy?,” *Phys. Rev. D* **80** (2009) 043530 [arXiv:0908.1333 [astro-ph.CO]].
- [30] S. Lee and K. W. Ng, “Spherical collapse model with non-clustering dark energy,” arXiv:0910.0126 [astro-ph.CO].
- [31] P. Creminelli, G. D’Amico, J. Norena, L. Senatore and F. Vernizzi, “Spherical collapse in quintessence models with zero speed of sound,” *JCAP* **1003** (2010) 027 [arXiv:0911.2701 [astro-ph.CO]].
- [32] F. Pace, J. C. Waizmann and M. Bartelmann, “Spherical collapse model in dark energy cosmologies,” arXiv:1005.0233 [astro-ph.CO].
- [33] N. Wintergerst and V. Pettorino, “Clarifying spherical collapse in coupled dark energy cosmologies,” arXiv:1005.1278 [astro-ph.CO].
- [34] W. Valkenburg, [arXiv:1104.1082 [gr-qc]].
- [35] A. Albrecht *et al.*, “Report of the Dark Energy Task Force,” arXiv:astro-ph/0609591.
- [36] P. J. E. Peebles, “Large-scale structure of the Universe,” Princeton University Press, Princeton NJ (1980).
- [37] S. Anselmi, G. Ballesteros and M. Pietroni, “Non-linear dark energy clustering,” arXiv:1106.0834 [astro-ph.CO].
- [38] D. Sapone, M. Kunz and M. Kunz, *Phys. Rev. D* **80** (2009) 083519 [arXiv:0909.0007 [astro-ph.CO]].
- [39] G. Ballesteros and J. Lesgourgues, “Dark energy with non-adiabatic sound speed: initial conditions and detectability,” arXiv:1004.5509 [astro-ph.CO].
- [40] W. H. Press and P. Schechter, “Formation of galaxies and clusters of galaxies by selfsimilar gravitational condensation,” *Astrophys. J.* **187** (1974) 425.
- [41] J. A. Peacock and A. F. Heavens, *Mon. Not. Roy. Astron. Soc.* **243** (1990) 133.
- [42] J. R. Bond, S. Cole, G. Efsthathiou and N. Kaiser, “Excursion set mass functions for hierarchical Gaussian fluctuations,” *Astrophys. J.* **379** (1991) 440.
- [43] M. Maggiori and A. Riotto, “The Halo Mass Function from the Excursion Set Method. I. First principle derivation for the non-markovian case of gaussian fluctuations and generic filter,” *Astrophys. J.* **711** (2010) 907 [arXiv:0903.1249 [astro-ph.CO]].
- [44] M. Maggiori and A. Riotto, “The halo mass function from the excursion set method. II. The diffusing barrier,” *Astrophys. J.* **717** (2010) 515 [arXiv:0903.1250 [astro-ph.CO]].
- [45] A. Ringwald and Y. Y. Y. Wong, “Gravitational clustering of relic neutrinos and implications for their detection,” *JCAP* **0412** (2004) 005 [arXiv:hep-ph/0408241].
- [46] E. Komatsu *et al.*, “Seven-Year Wilkinson Microwave Anisotropy Probe (WMAP) Observations: Cosmological Interpretation,” arXiv:1001.4538 [astro-ph.CO].
- [47] I. Maor and O. Lahav, “On virialization with dark energy,” *JCAP* **0507** (2005) 003 [arXiv:astro-ph/0505308].
- [48] P. Wang, “Virialization in Dark Energy Cosmology,” *Astrophys. J.* **640** (2006) 18 [arXiv:astro-ph/0507195].
- [49] C. P. Ma and E. Bertschinger, “Cosmological perturbation theory in the synchronous and conformal Newtonian gauges,” *Astrophys. J.* **455** (1995) 7 [arXiv:astro-ph/9506072].